Nanoscale

PAPER

View Article Online
View Journal | View Issue

Cite this: *Nanoscale*, 2017, **9**, 19353

Surface plasmon-enhanced amplified spontaneous emission from organic single crystals by integrating graphene/copper nanoparticle hybrid nanostructures†

Yun-Fei Li,[a] Jing Feng,*[a] Feng-Xi Dong,[a] Ran Ding,[a] Zhen-Yu Zhang,[a] Xu-Lin Zhang,[a] Yang Chen,[a] Yan-Gang Bi[a] and Hong-Bo Sun[a,b]

Received 10th September 2017,
Accepted 12th November 2017

DOI: 10.1039/c7nr06750j

rsc.li/nanoscale

Organic single crystals have attracted great attention because of their advantages such as high carrier mobility and high thermal stability. Amplified spontaneous emission (ASE) is an important parameter for the optoelectronic applications of organic single crystals. Here, surface plasmon-enhanced ASE from the organic single crystals has been demonstrated by integrating graphene/copper nanoparticle (Cu NP) hybrid nanostructures. Graphene is fully accommodating to the topography of Cu NPs by the transfer-free as-grown method for the configuration of the hybrid nanostructures, which makes full electrical contact and strong interactions between graphene and the local electric field of surface plasmon resonances. The enhanced localized surface plasmon resonances induced by the hybrid nanostructures result in an enhanced intensity and lowered threshold of ASE from the organic single crystals. Moreover, the as-grown graphene sheets covering fully and uniformly on the Cu NPs act as a barrier against oxidation, and results in an enhanced stability of the fluorescence from the crystals.

1 Introduction

Organic single crystals of π-conjugated oligomers are of increasing interest because of their applications in optoelectronics, such as organic solid-state lasers,[1–3] organic light-emitting devices (OLEDs),[4–6] organic field-effect transistors (OFETs),[7,8] and organic light-emitting field-effect transistors (OLEFETs).[9] The compact molecular packing and high chemical purity of crystals provide promising optical properties and charge carrier transport properties. For instance, they can emit light within the visible spectrum in a diode configuration, and can undergo population inversion at a low photopump intensity.[10,11] Amplified spontaneous emission (ASE) from the co-operative interaction among the aligned molecules of the organic crystals has been observed as the pump intensity increased above the threshold.[12–15] ASE is an important parameter for optoelectronic applications of organic crystals, especially, in a lasing process by characterizing the optical gain properties of the materials in-depth. Future implementation in optoelectronic devices urges more effective approaches to further enhance the light emission intensity, narrow the emission band and reduce the threshold of the ASE in organic crystals. Relevant efforts include the employment of a naturally cleaved facet as the Fabry–Pérot structures[16,17] and coupling of nanostructures using a thin film technology.[18–21] Surface plasmons (SPs) supported by the metallic nanostructures are known to dramatically modify the spontaneous emission of the nearby fluorescent molecules and materials and enhance the emission intensity by SP resonance. Lower threshold and stronger output intensity for lasing have been reported by a SP-enhanced gain in the dye film.[18–21] Enhanced ASE is expected by combining the metallic nanostructures with the crystals.

Among various metallic nanostructures, metallic nanoparticles (NPs) possess competitive advantages such as controllable synthesis[22–24] and ready integration into planar organic semiconductor waveguides. Localized surface plasmon resonances (LSPRs) supported by metallic NPs have been employed in optoelectronic devices to manipulate light generation and propagation.[25] Recently, it has been demonstrated that the LSPRs could be further enhanced by fabricating graphene/metallic NP hybrid nanostructures due to the graphene-induced improvements in the light–matter interactions.[26–28] Graphene/copper (Cu) NP hybrid nanostructures have been reported with simultaneous enhancement in both intensity

[a]State Key Laboratory of Integrated Optoelectronics, College of Electronic Science and Engineering, Jilin University, 2699 Qianjin Street, Changchun, 130012, People's Republic of China. E-mail: jingfeng@jlu.edu.cn
[b]State Key Lab of Precision Measurement and Instruments, Department of Precision Instrument, Tsinghua University, Haidian, Beijing, 100084, China

†Electronic supplementary information (ESI) available. See DOI: 10.1039/c7nr06750j

and stability of the LSPRs.[29] The hybrid nanostructures were easily fabricated with a one-step, etching and transfer-free method by directly growing graphene on the formed Cu NPs in the chemical vapor deposition (CVD) system. The configuration of the as-grown hybrid nanostructures, with graphene fully accommodating to the topography of copper nanoparticles, can provide full electrical contact and strong interactions between graphene and the local electric field of plasmon resonances.[30] In this study, the as-grown graphene/Cu NP hybrid nanostructures have been integrated with organic single crystals to achieve enhanced LSPRs and therefore enhanced ASE from the organic single crystals. With the introduction of the hybrid nanostructures, 2.5-fold enhanced emission intensity and 2 times lowered threshold were achieved compared to the organic single crystals with the bare Cu NPs. Moreover, the fluorescence exhibits much improved stability under ambient conditions on account of the graphene passivation.

2 Experimental details

2.1 Fabrication of graphene/Cu NP hybrid nanostructures

Copper strips (40 nm) were evaporated on the pre-cleaned quartz substrates at a base pressure of 5×10^{-4} Pa with a source of copper foil (Alfa Aesar, no. 46356). Then the samples were loaded into the center of a quartz tube, which was inserted inside the chemical vapor deposition (CVD) chamber, to fabricate Cu NPs and accommodate graphene at the temperature of 1000 °C under low partial pressure. The flow rates of CH_4, H_2, and Ar were 7, 30, and 200 standard cubic centimeters per minute (sccm), respectively. The temperature ramping rate was nearly 40 °C min^{-1}, followed by rapid cooling to room temperature (25 °C) with H_2 and Ar as protective gas configurations.

2.2 Preparation of BP3T single crystals

The powders of BP3T with the purity of 99% were purchased from the Kyoto Institute of Technology (KIT), and were employed without additional purification. Subsequently, the single crystals were prepared by an improved horizontal physical vapor transport method. The initial sublimation temperature of 405 °C and growth temperature of 365 °C inside the quartz tube were precisely controlled. A high-purity flowing argon stream was introduced as the carrier and protective gas, with the gas flow rate maintained at 38 mL min^{-1}. The grown single crystals were suspended on the growth tubes, and could be brought out by using tweezers easily. The thin crystals with high quality were then selected and transferred onto the substrates.

2.3 Emission characteristics

A pulse laser with a wavelength of 400 nm was employed as the pump source, which was obtained by the second harmonic generation of a regenerative amplifier (Solstice, Spectra Physics). Also, we introduced an attenuator wheel in the light path to adjust the pumping pulse energy as required. The dimension of the pumping laser spot on the samples was 1 mm in diameter. The emitted light was detected by optical fibers and then conveyed to a spectrometer.

3 Results and discussion

3.1 Preparation of BP3T on graphene/Cu NP hybrid nanostructures

Fig. 1a–d schematically illustrate the specific fabrication procedures of the single crystal of α,ω-bis(biphenyl)terthiophene (BP3T) integrated on the as-grown graphene/Cu NP hybrid nanostructures. Firstly, a copper strip with a thickness of 40 nm was prepared at the center of a pre-cleaned quartz substrate by thermal evaporation at a base pressure of 5×10^{-4} Pa. Thermal annealing was then performed in the low pressure chemical vapor deposition (LPCVD) system under an atmosphere of hydrogen (H_2) and argon (Ar) gas to obtain copper nanoparticles with morphology-controllable characteristics. After the introduction of methane (CH_4) gas into the chamber at the proper temperature of 1000 °C, graphene/copper nanoparticle hybrid nanostructures can be realized directly by rapid cooling without a time-consuming transfer method. It should be mentioned that this as-grown technique is convenient and well-suited for the mass production of the graphene–plasmonic hybrid nanostructures. Finally, the thin and flat single crystal materials, which were prepared by the improved physical vapor transport method with a flowing stream of argon,[31] were transferred onto the quartz substrate with half of the substrate coated with the graphene/copper nanoparticle hybrid nanostructures or bare Cu NPs. The fluorescence photograph of α,ω-bis(biphenyl)terthiophene (BP3T, see its chemical structure in Fig. 1e) under UV light irradiation is shown in Fig. 1f. As can be seen, BP3T is dominated by self-waveguided edge emission so that light is confined within the crystal and the fringes are brighter than the interior. This well-defined photoluminescence can be attributed to the transition dipole moments of the organic crystals in a nearly perpendicular configuration (Fig. 1g).

The morphological evaluations of the hemispherical Cu NPs coated with and without the as-grown graphene layers were performed by atomic force microscopy (AFM, Dimension Icon, Bruker Corporation) and transmission electron microscopy (TEM, JEM-2100F, JEOL) as shown in Fig. 2a–d, respectively. The average sizes of the graphene-coated and uncoated Cu NPs are determined to be about 600 nm in diameter, with the height featuring nearly 200 nm from statistical distribution. Notably, no apparent agglomeration or significant morphological changes occur at high temperature using methane gas as the carbon source in our as-grown technique. Fig. 2b reveals the successful growth of graphene on the outer shell of the Cu NPs with irregular edges. As we can see, the as-grown technique makes the contact between the growth layer and the Cu NPs smooth and seamless, which allows for strong interactions. Quality evaluation of the representative as-grown

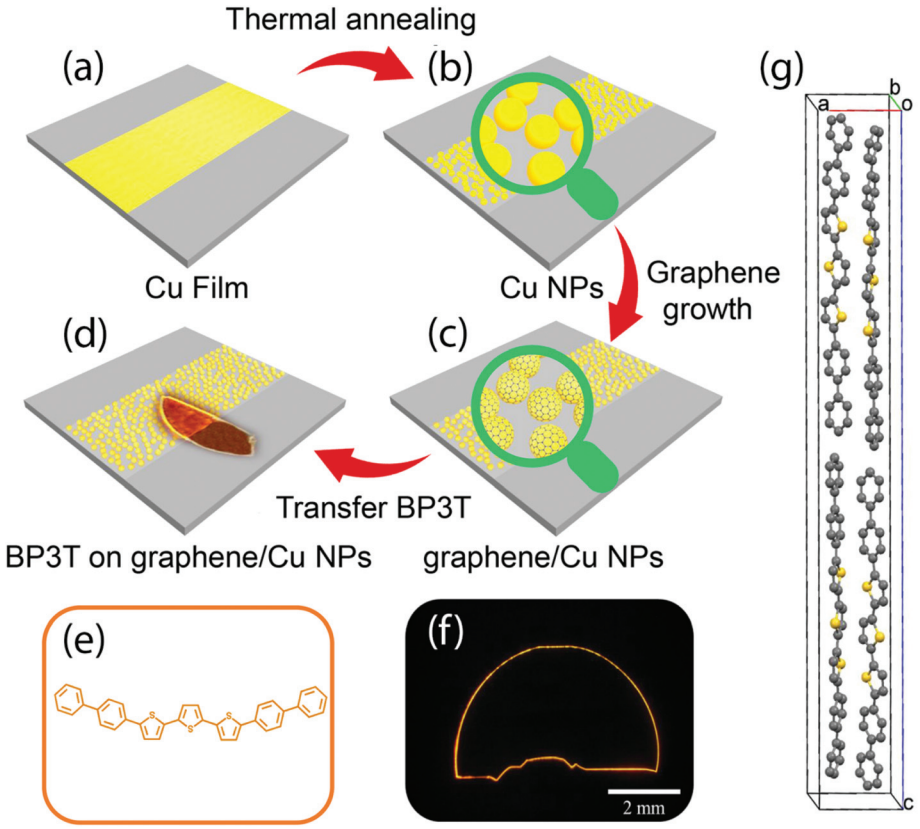

Fig. 1 (a)–(d) Schematics of the fabrication process for the as-grown graphene/Cu NP hybrid nanostructures. (e) The chemical structure of BP3T. (f) Fluorescence photograph of the BP3T crystal under UV light irradiation. (g) Crystal packing of BP3T.

graphene layers coated on Cu NPs was performed using the micro-Raman spectroscopy analysis (LabRAM HR Evolution Raman Spectrometer, Horiba Scientific) as shown in Fig. 2e. In order to get rid of the influence of Cu fluorescence peaks overlapping with the graphene peaks, the hybrid nanostructures were soaked in 20% HNO_3 for 10 h to etch the Cu cores prior to the Raman measurements. Three characteristic peaks can be clearly observed for the graphene layers corresponding to the D, G, and 2D bands, respectively. The intensity ratio of the 2D peak at 2695 cm^{-1} and the G peak at 1589 cm^{-1} is nearly 0.5, which indicates the formation of three-layer graphene. Moreover, the D peak at 1353 cm^{-1} appears in the disordered hexagonal sp^2 carbon network, probably arising from the finite particle-size effect, along with the strain-induced effects. Specifically, the as-grown graphene layers, fully accommodating to the topography of the Cu NPs, mainly range from 400 nm to 1 μm in diameter. Therefore, the obtained nanostructures are a bit smaller than the laser beam in size used in the Raman measurements, so that the bare quartz substrate area between the adjacent nanostructures could be regarded as defects. Besides this, the graphitic lattice was significantly stressed due to the high curvature of the hemispherical Cu NP surfaces. Due to the finite size and high stress of graphene, the D band is primarily considered as the unique structural deffects rather than the practical defects in the lattice, which will be further certified in the stability test. Furthermore, to provide insight into the specific function of graphene coupling to the SP resonances of Cu NPs, the extinction spectra for graphene/Cu NPs and bare Cu NPs were comparably examined and shown in Fig. 2f. Enhanced extinction can be observed from the graphene coated Cu NPs, which demonstrates the enhanced LSPRs induced by the introduction of graphene.

3.2 ASE characteristics of BP3T on graphene/Cu NP hybrid nanostructures

In order to investigate the effect of the as-grown graphene/Cu NP hybrid nanostructures on the optical properties of BP3T monolithic molecular crystals, the photoluminescence (PL) spectra of the BP3T with half of the crystals laminated onto the graphene/Cu NPs or Cu NPs are compared in Fig. 3a. Because the thickness of the organic crystals is crucial in their optical properties, we chose the BP3T single crystals with a similar thickness of nearly 200 nm for the comparison as shown in Fig. S1.† As expected, the BP3T single crystals based on the as-grown graphene/Cu NP hybrid nanostructures show obvious enhancement in the light emission intensity. Compared to the BP3T on the quartz substrate, an emission intensity of nearly 8.2-fold enhancement can be detected in the PL spectrum of the BP3T with the graphene/Cu NP hybrid nanostructures at a low pumping energy of 40.6 μJ cm^{-2}. The

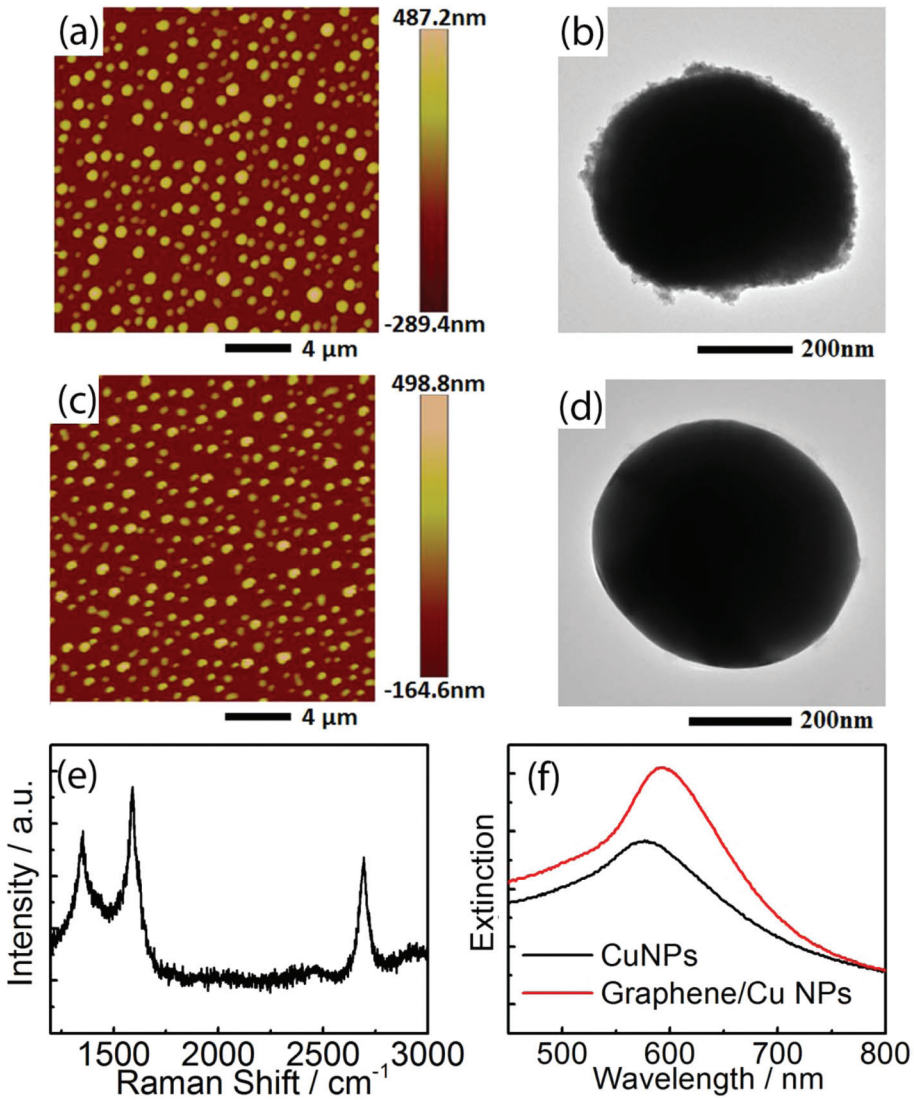

Fig. 2 AFM (a) and TEM (b) images of surface morphologies of graphene/Cu NP hybrid nanostructures, respectively. AFM (c) and TEM (d) images of surface morphologies of Cu NPs, respectively. (e) Raman spectrum of graphene in the hybrid nanostructures after removing Cu cores. (f) Extinction spectra for the Cu NPs with and without graphene coating.

BP3T single crystal laminated on the bare Cu NPs also presents an enhanced light emission intensity, while the enhancement factor is only 3.3.

Metallic NPs are known to dramatically modify the spontaneous emission of nearby fluorescent molecules by the SP-enabled near field coupling and result in the fluorescence enhancement. The time-correlated single-photon counting (TCSPC) was conducted to investigate the effect of the hybrid nanostructures on the spontaneous emission of BP3T crystals. As we can see from Fig. 3b, the intrinsic fluorescence decay lifetime of BP3T crystals with the thickness of 200 nm features at 3.48 ns, while the lifetime of the BP3T on graphene/Cu NPs and bare Cu NPs is 2.06 ns and 2.95 ns, respectively. Specific calculating procedures of the lifetime for BP3T single crystals are shown in Table S1.† It is noticeable that the graphene/Cu NP hybrid nanostructures considerably affect the spontaneous emission of BP3T by decreasing the lifetime. The shorter lifetime of the LSPR-tuned fluorescence is a physical phenomenon derived from the enhancement of the spontaneous emission rate which is caused by the stronger optical density of LSPRs at the interface. The graphene as grown on the Cu NPs allows a strong localization of the field at the graphene–copper interface and a dramatic field enhancement through LSPRs, especially with full electrical contact and strong interactions in the hybrid nanostructures. Therefore, the BP3T crystals on graphene/Cu NPs exhibit the shortest lifetime and the highest emission intensity. Also, we have presented the schematics of the band diagram of Cu–graphene–BP3T as shown in Fig. S2.†

The emission spectra of BP3T crystals with and without nanostructures were detected in the normal direction to the crystal planes with increasing pumping energy to investigate their ASE performance and are shown in Fig. 4. When increas-

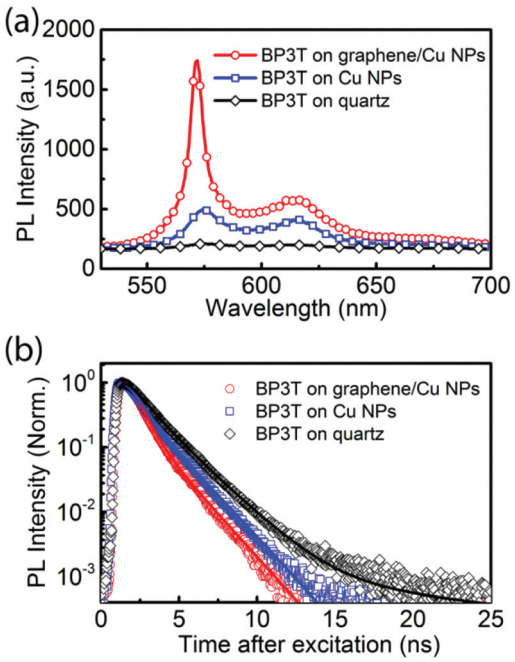

Fig. 3 PL spectra (a) and fluorescence lifetime (b) of the BP3T crystals on graphene/Cu NP hybrid nanostructures, bare Cu NPs and quartz, respectively.

ing the excitation pumping power above a certain threshold, the full width at half maximum (FWHM) of the BP3T decreases from 8.00 nm (on the quartz) to 6.24 nm (on the bare Cu NPs) and 5.20 nm (on the graphene/Cu NP hybrid nanostructures) as shown in Fig. 4a–c. In the meantime, the dependence of the FWHM and the PL peak intensity of emission for the crystals as a function of the incident laser pumping energy are summarized and shown in Fig. 4d. The threshold of the ASE for the BP3T with the Cu NPs decreased from 104.52 μJ cm^{-2} to 74.72 μJ cm^{-2}. The threshold of ASE for the BP3T integrated with the graphene/Cu NP hybrid nanostructures is determined to be 37.78 μJ cm^{-2}, which is nearly 3 times lower than that for the BP3T on the quartz substrate and 2 times lower than that for the BP3T on bare Cu NPs, respectively. A relevant study suggested that temperature could introduce certain impacts on the surface plasmon resonance of a given substance, *i.e.*, different optical responses may be observed at different temperatures.[32] Nevertheless, all experiments in this study were carried out under ambient conditions where we aim to extract information from the comparison between the samples under the same environmental conditions (*e.g.*, temperature).

3.3 Stability of BP3T on graphene/Cu NP hybrid nanostructures

On the other hand, the surface of pristine Cu NPs is chemically reactive and prone to oxidation with the formation of

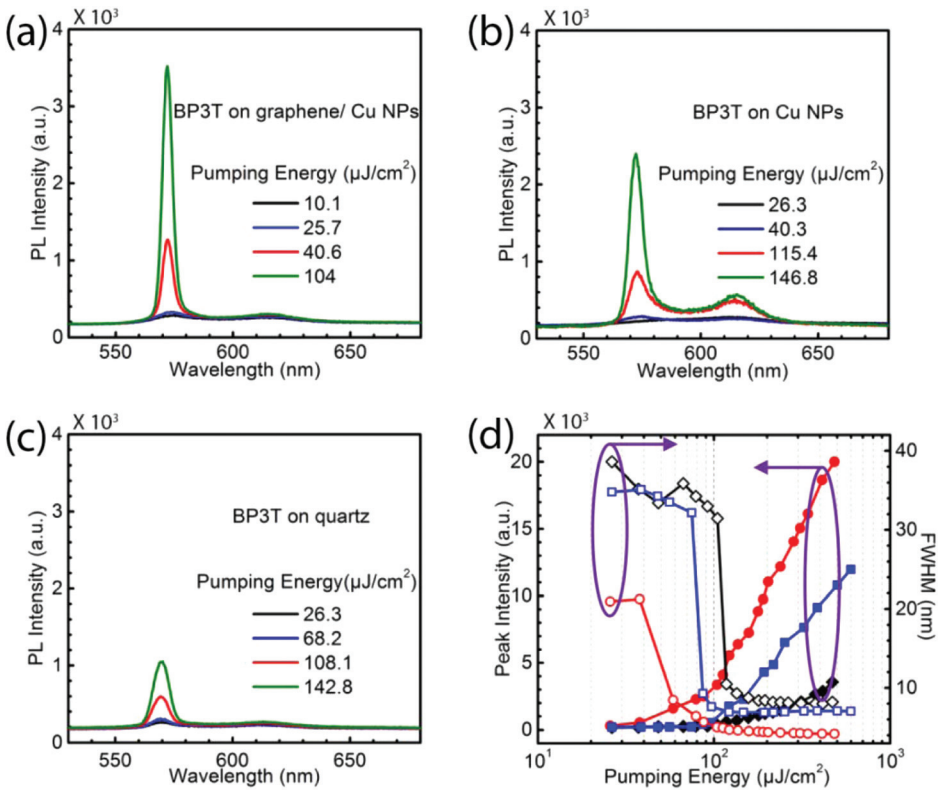

Fig. 4 PL spectra as a function of the pumping energy for BP3T crystals on graphene/Cu NPs (a), Cu NPs (b) and quartz (c). (d) Output peak intensity and FWHM as a function of the pumping energy for BP3T on graphene/Cu NPs (red), Cu NPs (blue) and quartz (black).

copper oxides when exposed to ambient air, leading to the undesirable degradation of the LSPRs.[33] Graphene in the hybrid nanostructures can function as a passivation layer to the copper surface without detrimental alteration to its physical properties.[34] The fluorescence stability of the BP3T modulated by the Cu NPs with and without the as-grown graphene under oxidation conditions was tested under ambient conditions with time evolution as shown in Fig. 5. As we can see, the PL intensity of the BP3T crystals remains stable with the increased exposure time on account of the characteristic of high thermal and chemical stabilities as shown in Fig. S3.† Meanwhile, the PL intensity of the BP3T crystal based on graphene/Cu NP hybrid nanostructures remains steady, with nearly unchanged light emission intensity after 7 days of exposure. In the case of BP3T on Cu NPs, the PL intensity declines dramatically after one week. The photographs of the BP3T under the illumination of a femtosecond pump beam have been taken to verify the effect of the nanostructures on the fluorescence and are shown in the insets of Fig. 5. Much brighter light emission can be observed from the half of the BP3T on the Cu NPs or hybrid nanostructures compared to the other half on the quartz substrate. Moreover, the emission from the BP3T on the hybrid nanostructures is brighter than that on the bare Cu NPs, which is consistent with the results shown in Fig. 3a. In particular, negligible variation of brightness can be observed for the BP3T integrated with the hybrid nanostructures after one week (insets of Fig. 5a). It is contrary to that of the BP3T with the bare Cu NPs, in which obvious degradation of luminescence can be seen in one week (insets of Fig. 5b). The much improved stability of the emission properties of the BP3T with the graphene/Cu NP hybrid nanostructures is attributed to the improved stability of the LSPRs of the hybrid nanostructures due to the effective passivation of the graphene on the Cu NPs.

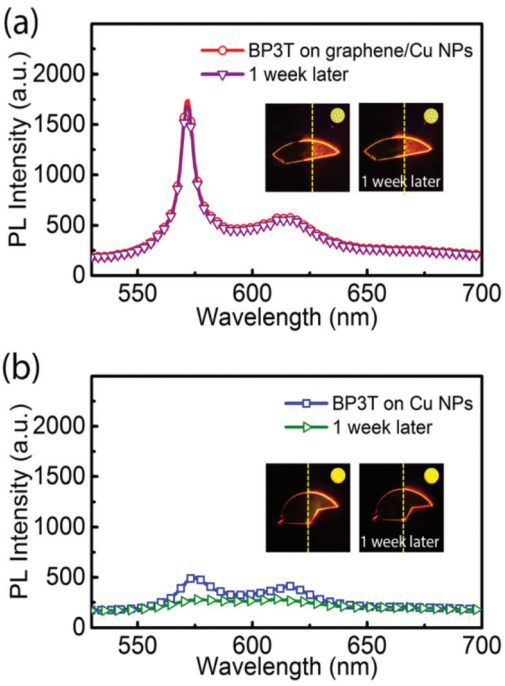

Fig. 5 Time evolution of PL spectra for the BP3T crystals with graphene/Cu NP hybrid nanostructures (a) and bare Cu NPs (b). Insets: Fluorescence photographs of BP3T crystals with the left half on the quartz and the right half on graphene/Cu NP hybrid nanostructures (insets of (a)) or bare Cu NPs (insets of (b)).

4 Conclusions

In conclusion, the as-grown graphene/Cu NP hybrid nanostructures have been integrated with the BP3T organic crystals to demonstrate the LSPR-enhanced ASE. The hybrid nanostructures with the introduction of graphene coating on the Cu NPs result in enhanced LSPRs, and the ASE threshold for the BP3T incorporated into the hybrid nanostructures is nearly two times lowered from 74.72 μJ cm^{-2} to 37.78 μJ cm^{-2} compared to that of the BP3T with the bare Cu NPs. In addition, the passivation of graphene on the Cu NPs is beneficial for the stability of the fluorescence of BP3T, and no obvious fluorescence degradation can be observed in one week. The much improved emission properties of the organic single crystals by integrating with the graphene/Cu NP hybrid nanostructures provide an effective approach to promote the development of organic single crystal-based electric and optoelectronic devices for practical applications.

Conflicts of interest

There are no conflicts to declare.

Acknowledgements

The authors gratefully acknowledge financial support from the National Key Research and Development Program of China (Project No. 2017YFB0404501) and NSFC (Grant No. 61675085, 61705075, 61590930 and 51373064).

References

1 M. Ichikawa, R. Hibino, M. Inoue, T. Haritani, S. Hotta, K. Araki, T. Koyama and Y. Taniguchi, *Adv. Mater.*, 2005, **17**, 2073–2077.
2 H. Fang, J. Yang, J. Feng, T. Yamao, S. Hotta and H. Sun, *Laser Photonics Rev.*, 2014, **8**, 687–715.
3 R. Ding, H. Fang, Y. Wang, S. Lu, X. Zhang, L. Wang, J. Feng, Q. Chen and H. Sun, *Org. Electron.*, 2012, **13**, 1602–1605.
4 R. Ding, J. Feng, X. Zhang, W. Zhou, H. Fang, Y. Liu, Q. Chen, H. Wang and H. Sun, *Adv. Funct. Mater.*, 2014, **24**, 7085–7092.
5 M. Ichikawa, K. Nakamura, M. Inoue, H. Mishima, T. Haritani, R. Hibino, T. Koyama and Y. Taniguchi, *Appl. Phys. Lett.*, 2005, **87**, 221113.

6 H. Yanagi, T. Morikawa and S. Hotta, *Appl. Phys. Lett.*, 2002, **81**, 1512–1514.
7 H. Nakanotani, M. Saito, H. Nakamura and C. Adachi, *Appl. Phys. Lett.*, 2009, **95**, 033308.
8 T. Katagiri, Y. Shimizu, K. Terasaki, T. Yamao and S. Hotta, *Org. Electron.*, 2011, **12**, 8–14.
9 H. Wang, F. Li, I. Ravia, B. Gao, Y. Li, V. Medvedev, H. Sun, N. Tessler and Y. Ma, *Adv. Funct. Mater.*, 2011, **21**, 3770–3777.
10 J. R. Sheats, H. Antoniadis, M. Hueschen, W. Leonard, J. Miller, R. Moon, D. Roitman and A. Stocking, *Science*, 1996, **27**, 885–888.
11 A. Dodabalapur, *Solid State Commun.*, 1997, **102**, 259–267.
12 H. Cao, J. Y. Xu, S. Chang and S. T. Ho, *Phys. Rev. E: Stat. Phys., Plasmas, Fluids, Relat. Interdiscip. Top.*, 2000, **61**, 1985–1989.
13 K. Kim, *Phys. Rev. Lett.*, 1986, **57**, 1871–1874.
14 M. D. McGehee, R. Gupta, S. Veenstra, E. K. Miller, M. A. Diaz-Garcia and A. J. Heeger, *Phys. Rev. B: Condens. Matter Mater. Phys.*, 1998, **58**, 7035–7039.
15 T. Hiramatsu, N. Matsuoka, H. Yanagi, F. Sasaki and S. Hotta, *Phys. Status Solidi RRL*, 2009, **6**, 338–341.
16 T. Yamao, K. Yamamoto, Y. Taniguchi, T. Miki and S. Hotta, *J. Appl. Phys.*, 2008, **103**, 093115.
17 M. Ichikawa, K. Nakamura, M. Inoue, H. Mishima, T. Haritani, R. Hibino, T. Koyama and Y. Taniguchi, *Appl. Phys. Lett.*, 2002, **87**, 221113.
18 G. Heliotis, R. Xia, G. A. Turnbull, P. Andrew, W. L. Barnes, I. D. W. Samuel and D. D. C. Bradley, *Adv. Funct. Mater.*, 2004, **14**, 91–97.
19 N. Tessler, G. J. Denton and R. H. Friend, *Nature*, 1996, **382**, 695–697.
20 D. O'Carroll, I. Lieberwirth and G. Redmond, *Nat. Nanotechnol.*, 2007, **56**, 180–184.
21 S. Riechel, C. Kallinger, U. Lemmer, J. Feldmann, A. Gombert, V. Wittwer and U. Scherf, *Appl. Phys. Lett.*, 2000, **77**, 2310–2312.
22 Y. H. Nishijima, Y. Hashimoto, L. Rosa, J. B. Khurgin and S. Juodkazis, *Adv. Opt. Mater.*, 2014, **2**, 382–388.
23 Y. Lin and D. P. Tsai, *Opt. Express*, 2012, **20**, 16205–16211.
24 L. C. Cheng, H. M. Chen, T. C. Lai, Y. C. Chan, R. S. Liu, J. C. Sung, M. Hsiao, C. H. Chen, L. J. Herf and D. P. Tsai, *Nanoscale*, 2013, **5**, 3931–3940.
25 H. Y. Chung, P. T. Leung and D. P. Tsai, *Opt. Express*, 2013, **21**, 26483–26492.
26 X. Zhu, L. Shi, M. S. Schmidt, A. Boisen, O. Hansen, J. Zi, S. Xiao and N. A. Mortensen, *Nano Lett.*, 2013, **13**, 4690–4696.
27 (*a*) X. Chen, B. Jia, Y. Zhang and M. Gu, *Light: Sci. Appl.*, 2013, **2**, e92; (*b*) Z. Zheng, J. Li, T. Ma, H. Fang, W. Ren, J. Chen, J. She, Y. Zhang, F. Liu, H. Chen, S. Deng and N. Xu, *Light: Sci. Appl.*, 2017, **6**, e17057.
28 S. Zeng, K. V. Sreekanth, J. Shang, T. Yu, C. Chen, F. Yin, D. Baillargeat, P. Coquet, H. Ho, A. V. Kabashin and K. Yong, *Adv. Mater.*, 2015, **27**, 6163–6169.
29 Y. Li, F. Dong, Y. Chen, X. Zhang, L. Wang, Y. Bi, Z. Tian, Y. Liu, J. Feng and H. Sun, *Sci. Rep.*, 2016, **6**, 37190.
30 S. Lee, J. Hong, J. H. Koo, H. Lee, S. Lee, T. Choi, H. Jung, B. Koo, J. Park, H. Kim, Y. Kim and T. Lee, *ACS Appl. Mater. Interfaces*, 2013, **5**, 2432–2437.
31 R. Ding, J. Feng, W. Zhou, X. Zhang, H. Fang, T. Yang, H. Wang, S. Hotta and H. Sun, *Sci. Rep.*, 2015, **5**, 12445.
32 H. P. Chiang, H. T. Yeh, C. M. Chen, J. C. Wu, S. Y. Su, R. Chang, Y. J. Wu, D. P. Tsai, S. U. Jen and P. T. Leung, *Opt. Commun.*, 2004, **241**, 409–418.
33 K. Sugawa, T. Tamura, H. Tahara, D. Yamaguchi, T. Akiyama, J. Otsuki, Y. Kusaka, N. Fukuda and H. Ushijima, *ACS Nano*, 2013, **7**, 9997–10010.
34 S. Wang, X. Huang, Y. He, H. Huang, Y. Wu, L. Hou, X. Liu, T. Yang, J. Zou and B. Huang, *Carbon*, 2012, **50**, 2119–2125.